EPJ Web of Conferences **119**, 01004 (2016) DOI: 10.1051/epjconf/201611901004
ILRC 27

HETEAC: THE AEROSOL CLASSIFICATION MODEL FOR EARTHCARE

Ulla Wandinger[1]*, Holger Baars[1], Ronny Engelmann[1], Anja Hünerbein[1], Stefan Horn[1], Thomas Kanitz[1,4], David Donovan[2], Gerd-Jan van Zadelhoff[2], David Daou[2], Jürgen Fischer[3], Jonas von Bismarck[3], Florian Filipitsch[3], Nicole Docter[3], Michael Eisinger[4], Dulce Lajas[4], Tobias Wehr[4]

[1]*Leibniz Institute for Tropospheric Research (TROPOS), Leipzig, Germany, *Email: ulla@tropos.de*

[2] *Royal Netherlands Meteorological Institute (KNMI), De Bilt, The Netherlands*

[3]*Free University of Berlin (FUB), Institute for Space Science, Berlin, Germany*

[4]*European Space Agency (ESA), European Space Research and Technology Centre (ESTEC), Noordwijk, The Netherlands*

ABSTRACT

We introduce the Hybrid End-To-End Aerosol Classification (HETEAC) model for the upcoming EarthCARE mission. The model serves as the common baseline for development, evaluation, and implementation of EarthCARE algorithms. It shall ensure the consistency of different aerosol products from the multi-instrument platform as well as facilitate the conform specification of broad-band optical properties necessary for the EarthCARE radiative closure efforts. The hybrid approach ensures the theoretical description of aerosol microphysics consistent with the optical properties of various aerosol types known from observations. The end-to-end model permits the uniform representation of aerosol types in terms of microphysical, optical and radiative properties.

1. INTRODUCTION

The Earth Clouds, Aerosols and Radiation Explorer (EarthCARE) is a joint ESA/JAXA mission planned to be launched in 2018 [1]. The multi-sensor platform comprises a cloud-profiling radar (CPR), a high-spectral-resolution cloud/aerosol lidar (ATLID), a cloud/aerosol multi-spectral imager (MSI), and a three-view broad-band radiometer (BBR). Three out of the four instruments (ATLID, MSI, and BBR) will be able to sense the global aerosol distribution and contribute to the overarching EarthCARE goals of sensor synergy and radiation closure with respect to aerosols.

The high-spectral-resolution lidar ATLID obtains profiles of particle extinction and backscatter coefficients, lidar ratio, and linear depolarization ratio as well as the aerosol optical thickness (AOT) at 355 nm along the track of the satellite. The MSI provides AOT at 670 nm (over land and ocean) and 865 nm (over ocean) across a 150-km wide swath. From combined ATLID and MSI data, the columnar Ångström exponent for the 355/670/865-nm spectral range can be inferred along track.

MSI observations will also be used to extend the two-dimensional cross-sections from lidar and radar into the three-dimensional domain, which then will serve as input to broadband radiative-transfer models [2]. In this way, fluxes, heating rates, and radiances can be calculated and top-of-atmosphere (TOA) radiances and fluxes compared to those derived from BBR measurements. The aim is to reach closure of measured and calculated TOA fluxes over each 10 km by 10 km scene with an accuracy of 10 Wm^{-2}, with the final goal to substantially decrease the uncertainties in our knowledge of global radiative forcing.

With respect to aerosols, the closure studies require a proper aerosol classification so that microphysical properties such as particle size (effective radius) or scattering and absorption efficiencies (single-scattering albedo) can be assigned to predefined aerosol types, which in turn can be identified from the measurements of their optical properties. Aerosol classification from space-borne observations is also required for quantification of anthropogenic versus natural aerosol loadings of the atmosphere, investigation of aerosol-cloud interaction, as well as assimilation purposes and validation of atmospheric transport models which carry components like dust, sea salt, smoke and pollution.

In order to facilitate a common aerosol classification and the consistency of all EarthCARE aerosol products, the Hybrid End-to-End Aerosol Classification (HETEAC) model is being developed. The model is based on a combined experimental and theoretical, i.e. hybrid, approach and allows the end-to-end simulation of aerosol properties, from microphysical to optical and radiative parameters of predefined aerosol types. In the following, we describe the basic considerations and the current development steps in more detail. Section 2 gives an overview of the classification approach. Sec. 3 shows the experimental basis for the EarthCARE typing scheme, and Sec. 4 presents a first attempt of the simulation of

microphysical properties. An outlook on the next steps of HETEAC developments is given in Sec. 5.

2. AEROSOL CLASSIFICATION SCHEMES

Different approaches for aerosol classification are available in the literature. For HETEAC, the heritage of previous attempts is considered, while at the same time the specific observing capabilities of the mission are taken into account.

Previous aerosol classification schemes rely on experimental findings from passive and active remote sensing and use specific "optical footprints" primarily based on intensive, i.e. concentration-independent, optical properties but also on aerosol load, geographic location or altitude of occurrence. Such schemes have been developed in the context of the CALIPSO mission [3, 4], derived from dedicated lidar field studies [5, 6] or retrieved from passive remote-sensing observations [7].

Usually, the classification schemes distinguish three groups of aerosol types: 1) so-called pure types like marine, smoke, pollution or dust aerosols, 2) mixtures of the former types, and 3) aerosol types that occur only in specific locations like the polar region or the stratosphere. A common understanding exists to define pure types of desert dust, marine aerosol and anthropogenic pollution. These types can usually be well discriminated due to their well-defined and clearly different optical appearance. Biomass-burning aerosol or smoke is an important player as well, but differently treated due to its variable nature. The optical and microphysical properties of smoke can be quite different depending on the kind of burnt material (e.g., Savannah or boreal fires, crop burning), the kind of burning (smoldering or flaming) and the time of transport (atmospheric processing of particles). There are also different ways to account for aerosol mixtures, e.g., mixtures of dust with biomass-burning, marine or pollution aerosols or mixtures of marine and pollution aerosols.

In the CALIPSO retrievals six aerosol types, i.e. clean marine, clean continental, polluted continental, dust, polluted dust, and biomass-burning smoke, are distinguished. CALIPSO aerosol typing relies on lidar level-1 data, since the methodology has been developed primarily to select proper lidar ratios for level-2 data retrievals. Thus, selection criteria comprise integrated attenuated backscatter, approximated depolarization ratio, and vertical location of the layer as well as the kind of surface above which the observation is made.

The EarthCARE aerosol classification scheme shall preserve the aerosol types of CALIPSO as far as possible in order to allow long-term global investigations over the lifetime of both missions. However, a more robust typing based on level-2 data will be applied. Due to the high-spectral-resolution lidar approach, ATLID retrievals do not require an *a priori* estimate of the particle lidar ratio, but provide this quantity together with the particle linear depolarization ratio as an observable. EarthCARE's aerosol-type product can thus rely on measured intensive, i.e. concentration-independent, particle properties. ATLID observations are performed at 355 nm. Up to now, there is no specific aerosol typing scheme available that considers a classification based on measurements at this wavelength. Therefore, as a first step, the experimental basis of aerosol typing at 355 nm must be established.

3. EXPERIMENTAL BASIS

Figure 1 shows a collection of ground-based observations of lidar ratio and particle linear depolarization ratio at 355 nm from several field campaigns in different locations of the world. The different aerosol types (dust, smoke, pollution, marine aerosol, volcanic ash) and mixtures of them spread in this 2D-representation of intensive particle properties that will be measured with ATLID. It is obvious that a clear distinction between small, absorbing particles (high lidar ratio, small depolarization ratio = smoke or pollution), large spherical particles (small lidar ratio, small depolarization ratio = marine aerosol), and large non-spherical particles (moderate to high lidar ratio, high depolarization ratio = dust or ash) is possible. Mixtures of these types appear with intermediate values of lidar ratio and depolarization ratio. Thus, some estimate of the mixing state will be possible as well. Based on these findings, the next step is to find appropriate microphysical descriptions for the aerosol types that are consistent with the observations.

4. SIMULATION OF MICROPHYSICAL PROPERTIES

Starting with a very simple approach for the microphysical description, we assign a mono-modal particle size distribution and a (wavelength-dependent) complex refractive index to well-known basic aerosol components. Here, we follow the attempt of the aerosol project within the ESA Climate Change Initiative (Aerosol_cci) which focusses on the investigation of retrieval algorithms and products from passive satellite remote sensing. For the retrieval experiments an aerosol model based on four components is used [8]. These components comprise two fine modes, one strongly absorbing and one weakly absorbing, and two coarse modes, one with spherical particles representing sea salt and one with non-spherical particles representing dust. The mode radii and refractive

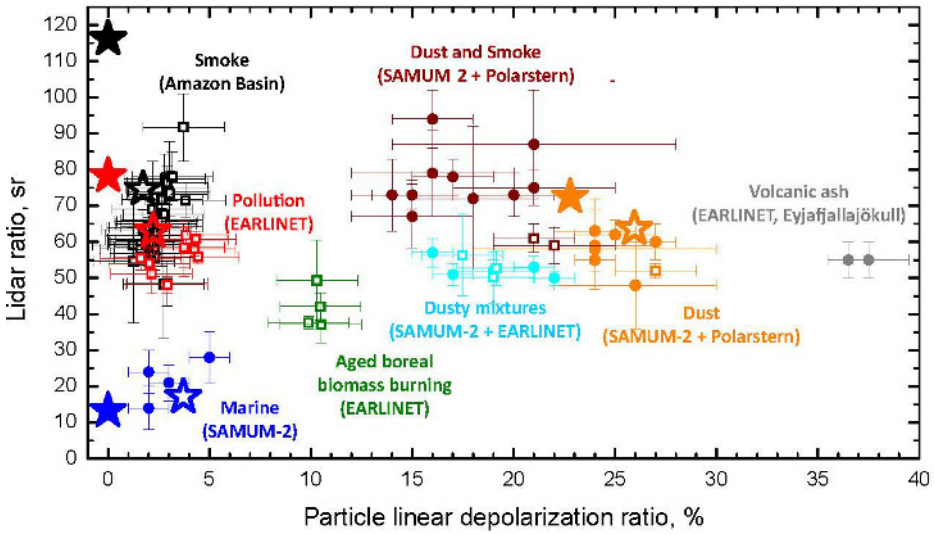

Figure 1: Ground-based observations and simulations of lidar ratio versus particle linear depolarization ratio at the ATLID wavelength of 355 nm. Measurements were performed with the Raman-polarization lidars POLIS (University of Munich, dots) and Polly^{XT} (Leibniz Institute for Tropospheric Research, open squares) during SAMUM-2 at Cape Verde [9], at the EARLINET stations of Leipzig and Munich, Germany [10], in the Amazon Basin [11], and onboard Polarstern over the North Atlantic [12]. Simulations were performed using the components of Aerosol_cci (filled stars) and variations with different refractive index and shape distribution (open stars).

indexes are typical values obtained from long-term AERONET observations (see Table 1).

Table 1: Microphysical properties of the components of the Aerosol_cci model and their optical properties at 355 nm. Italic numbers represent a variation that reproduces observational findings for Saharan dust, marine aerosol, pollution, and smoke (r_{eff}–effective radius, m_R–refractive index, real part, m_I–refractive index, imaginary part, S–lidar ratio, δ–particle linear depolarization ratio, ω_0–single-scattering albedo).

	Coarse mode: Dust	Coarse mode: Sea salt	Fine mode: Weakly absorbing	Fine mode: Strongly absorbing
r_{eff}, µm	1.94	1.94	0.14	0.14
m_R	1.56 *1.53*	1.40 *1.36*	1.40 *1.45*	1.50 *1.55*
m_I	0.005 *0.003*	0.0	0.003	0.043 *0.030*
Shape	Dubovik's spheroid distribution	Spherical *10% prolates with axis ratio 1.1*	Spherical *100% prolates with axis ratio 1.1*	Spherical *100% prolates with axis ratio 1.1*
S, sr	72.5, *63.7*	13.3 *17.1*	78.3 *63.0*	116.9 *74.6*
δ, %	22.8 *26.0*	0.0 *3.7*	0.0 *2.2*	0.0 *1.7*
ω_0	0.81 *0.87*	1.00 *1.00*	0.98 *0.98*	0.81 *0.86*

In order to describe the scattering of non-spherical particles, we apply the spheroid model and the spheroid shape distribution (mixture of prolates and oblates with axis ratios between 0.3 and 3) introduced by Dubovik et al. [13]. Figure 1 shows the values of lidar ratio and linear depolarization ratio calculated for the Aerosol_cci components at 355 nm (filled stars). It can be seen that these components already relatively well represent the properties of Saharan dust (non-spherical coarse mode), sea salt (spherical coarse mode), pollution (weakly absorbing fine mode) and smoke (strongly absorbing fine mode). Some variation of the refractive-index values and the content of non-spherical particles (see italic numbers in Table 1) shifts the theoretically calculated values close to the experimental ones (see open stars in Fig. 1).

5. NEXT STEPS

Starting from these promising results, the microphysical model will be further refined. In particular, we will combine the Aerosol_cci approach with the Optical Properties of Aerosols and Clouds (OPAC) database [14, 15]. OPAC allows the construction of aerosol types from a number of basic aerosol components with well-defined microphysical properties under consideration of hygroscopic particle growth, and it provides a comprehensive collection of refractive indexes of basic aerosol components over a wide wavelength range (0.25–40 µm). The latter is needed for the radiative-transfer calculations and the closure studies with BBR. In the new OPAC 4.0, three dust components (nucleation, accumulation, and coarse mode) are contained which are made up of non-spherical scatterers of prolate shape. A size-dependent axis-ratio distribution following experimental results

obtained by Kandler et al. [16] is considered. Our first investigations show that this shape distribution better represents the experimental data than the one proposed by Dubovik et al. [13].

The experimental basis will be extended as well in order to consider the spectral behavior of extinction, backscatter and depolarization. The corresponding Ångström exponents are taken from multi-wavelength Raman lidar observations. Respective information for many of the observations shown in Fig. 1 is already available and more experimental data will be included. The consistency of the aerosol model over the entire ATLID/MSI wavelength range can be assured in this way. The HETEAC pure and mixed aerosol types shall finally be constructed from bi-modal size distributions representing the contribution of fine and coarse particles of different complex refractive index and with different shape distributions.

ACKNOWLEDGEMENT

The work presented in this paper is performed within the project Atmospheric Products from Imager and Lidar (APRIL) funded by ESA under contract 4000112018/14/NL/CT.

REFERENCES

[1] Illingworth, A., et al., 2014: THE EARTHCARE SATELLITE: The next step forward in global measurements of clouds, aerosols, precipitation and radiation. *Bull. Am. Met. Soc.*, doi:10.1175/BAMS-D-12-00227.1.

[2] Barker, H. W., et al., 2011: A 3D cloud-construction algorithm for the EarthCARE satellite mission. *Q. J. R. Meteorol. Soc.*, **137**, 1042–1058, doi: 10.1002/qj.824.

[3] Omar, A. H., et al., 2005: Development of global aerosol models using cluster analysis of Aerosol Robotic Network (AERONET) measurements, *J. Geophys. Res.*, **110**, D10S14, doi:10.1029/2004JD 004874.

[4] Omar, A. H., et al., 2009: The CALIPSO automated aerosol classification and lidar ratio selection algorithm. *J. Atmos. Oceanic Technol.*, **26**, 1994–2014. doi:10.1175/2009JTECHA1231.1.

[5] Burton, S. P., et al., 2012: Aerosol classification using airborne High Spectral Resolution Lidar measurements – methodology and examples. *Atmos. Meas. Tech.*, **5**, 73–98, doi:10.5194/amt-5-73-2012.

[6] Groß, S., et al., 2014: Towards an aerosol classification scheme for future EarthCARE lidar observations and implications for research needs. *Atmosph. Sci. Lett.*, **16**, 77–82, doi: 10.1002/asl2.524.

[7] Russell, P. B., et al., 2014: A multiparameter aerosol classification method and its application to retrievals from spaceborne polarimetry. *J. Geophys. Res. Atmos.*, **119**, 9838–9863, doi:10.1002/2013JD 021411.

[8] Holzer-Popp, T., et al., 2013: Aerosol retrieval experiments in the ESA Aerosol_cci project, *Atmos. Meas. Tech.*, **6**, 1919–1957, doi:10.5194/amt-6-1919-2013.

[9] Groß, S., et al., 2011: Characterization of Saharan dust, marine aerosols and mixtures of biomass-burning aerosols and dust by means of multi-wavelength depolarization and Raman lidar measurements during SAMUM 2. *Tellus B*, **63**, 706–724, doi:10.1111/j.1600-0889.2011.00556.x.

[10] Groß, S., et al., 2012: Dual-wavelength linear depolarization ratio of volcanic aerosols: Lidar measurements of the Eyjafjallajökull plume over Maisach, Germany. *Atm. Env.*, **48**, 85–96, doi:10.1016/j.atmosenv.2011.06.017.

[11] Baars, H., et al., 2012: Aerosol profiling with lidar in the Amazon Basin during the wet and dry season. *J. Geophys. Res.,* **117**, D21201, doi:10.1029/2012JD 018338.

[12] Kanitz, T., et al., 2013: North-south cross sections of the vertical aerosol distribution over the Atlantic Ocean from multiwavelength Raman/polarization lidar during Polarstern cruises. *J. Geophys. Res. Atmos.*, **118**, 2643–2655, doi:10.1002/jgrd.50273.

[13] Dubovik, O., et al., 2006: Application of spheroid models to account for aerosol particle nonsphericity in remote sensing of desert dust. *J. Geophys. Res.*, **111**, D11208, doi:10.1029/2005JD006619.

[14] Hess, M., et al., 1998a: Optical properties of aerosols and clouds: The software package OPAC. *Bull. Am. Met. Soc.*, **79**, 831–844.

[15] Koepke, P., et al., 2015: Technical Note: Optical properties of desert dust with non-spherical particles: data incorporated to OPAC. *Atmos. Chem. Phys. Discuss.*, **15**, 3995–4023, doi:10.5194/acpd-15-3995-2015.

[16] Kandler, K., et al., 2009: Size distributions, mass concentrations, chemical and mineralogical composition, and derived optical parameters of the boundary layer aerosol at Tinfou, Morocco, during SAMUM 2006, *Tellus B*, **61**, 32–50, doi:10.1111/j.1600-0889.2008.00385.x.